ORIGINAL ARTICLE

WILEY   mycoses
Diagnosis, Therapy and Prophylaxis of Fungal Diseases

Performance of magnetic resonance imaging in pulmonary fungal disease compared to high-resolution computed tomography

Ana Sartori[1] | Arthur Souza[2] | Matheus Zanon[1,3] (iD) | Klaus Irion[4] | Edson Marchiori[2] | Guilherme Watte[1] | Bruno Hochhegger[1,3]

[1]LABIMED – Medical Imaging Research Lab, Department of Radiology, Pavilhão Pereira Filho Hospital, Irmandade Santa Casa de Misericórdia de Porto Alegre, Porto Alegre, Brazil

[2]Federal University of Rio de Janeiro, Rio de Janeiro, Brazil

[3]Federal University of Health Sciences of Porto Alegre, Porto Alegre, Brazil

[4]Manchester Royal Infirmary, Central Manchester University Hospitals, Manchester, UK

Correspondence
Matheus Zanon, LABIMED – Medical Imaging Research Lab, Department of Radiology, Pavilhão Pereira Filho Hospital, Irmandade Santa Casa de Misericórdia de Porto Alegre, Porto Alegre, Brazil.
Email: mhgzanon@hotmail.com

Summary

To evaluate the performance of magnetic resonance imaging (MRI) compared to computed tomography (CT) in patients diagnosed with pulmonary mycosis. We prospectively included 21 patients diagnosed with pulmonary mycosis between January 2013 and October 2014. Inclusion criteria were presence of respiratory symptoms, histopathological diagnosis of mycosis and absence of mycosis treatment. Reviewers identified one predominant imaging pattern per patient: nodular, reticular or airspace pattern. Afterwards, all CT findings were analysed separately per lobe and compared to MRI. Nodular pattern was the most common found (CT: 76.20%; MRI: 80.96%), followed by airspace pattern (CT and MRI: 9.52%) and reticular (CT: 9.52%; MRI: 4.76%). Compared to CT, MRI performance varied according to radiological finding and pulmonary region. For nodules, MRI presented high sensitivity (100% [95% CI: 93.52-100]) and specificity (100% [95% CI: 92.00-100]). For bronchiectasis and septal thickening, there were poorer positive predictive values (33.33% [95% CI: 1.77-87.47]; and 83.33% [95% CI: 50.88-97.06] respectively). As specificity and negative predictive value had superior results than sensitivity and positive predictive value, rather than for diagnosis of this condition, MRI might be more considered for the follow-up of patients with pulmonary mycosis, an alternative to multiple radiation exposures with CT follow-up.

KEYWORDS
computed tomography, diffusion-weighted imaging, magnetic resonance imaging, mycosis, pulmonary fungal disease

1 | INTRODUCTION

Fungal infection is a growing cause of lung disease worldwide, related to the large number of immunocompromised patients and to the growth of populations in endemic areas. Lung mycosis is usually self-limited, but some patients develop chronic infection. The main clinical issue related to this infection is the lack of criteria to define a healed status, which, in some cases, can lead to an unnecessary follow-up for many years with chest computed tomography (CT), creating a concern related to high radiation exposure.[1] High-resolution computed tomography (HRCT) is the gold standard for the diagnosis and follow-up of lung mycosis.[2] As the clinical manifestations of fungal diseases are non-specific and similar to those of other infections, radiology plays a crucial role on their diagnosis.[2] Although imaging can often be non-specific as well, fungal infection usually manifests as airspace disease, characterised by features such as consolidation and ground-glass opacity (GGO), nodules and micronodules, masses, airway disease (eg bronchial thickening and bronchiectasis), fibroatelectatic lesions and interlobular septal thickening.[3–7]

Pulmonary magnetic resonance imaging (MRI) has been introduced as a new diagnostic tool in parenchymal evaluation, with the great advantage of non-use of ionising radiation.[8] Advances in equipment, shortening of sequence acquisition times and the availability of respiratory gates have improved image quality, enabling the evaluation of lung parenchyma.[9] MRI has been used to study many lung diseases, such as sarcoidosis, cancer, cystic fibrosis, and pulmonary fibrosis, with good results and strong correlation with CT findings.[10–12] Diffusion-weighted imaging (DWI), based on the differential mobility of water molecules (Brownian motion) in tissues, generates quantitative (apparent diffusion coefficient) and qualitative (signal strength) data reflecting changes at the cellular level, which provide information about tumour cellularity and cell membrane integrity.[13] Recent studies have demonstrated the potential of this modality to differentiate malignant from benign pulmonary nodules.[13] However, no recent study has explored the use of MRI with DWI for the assessment of fungal disease.

Given the increase in accumulated radiation exposure due to long-term follow-up, we primarily sought to demonstrate the utility of MRI for the evaluation of pulmonary mycosis compared to high-resolution CT, describing the DWI findings for this disease.

2 | MATERIALS AND METHODS

With the approval of our institutional review board and written informed consent, this prospective study included data from all patients diagnosed with fungal disease in two hospitals between January 2013 and October 2014. Inclusion criteria were respiratory symptoms (dyspnoea, tachypnoea or cough), histopathological diagnosis of mycosis by bronchoalveolar lavage (BAL) or lung biopsy, and performance of HRCT at the time of diagnosis. All patients underwent chest MRI on same day as CT examination. As DWI signal and findings might differ in patients under treatment due to cell oedema and apoptosis, we only included treatment-free patients.[10,11] Exclusion criteria were claustrophobia and clinical inability to undergo the examination.

2.1 | Patients

Study subjects' demographic characteristics are summarised in Table 1. The study sample comprised 21 patients (17 men and four women) with a mean age of 58.1 (range, 32-80) years who were diagnosed with paracoccidioidomycosis (n=11), histoplasmosis (n=4), cryptococcosis (n=4) and *Aspergillus* infection (n=2) and met the inclusion criteria. Two patients were excluded from the study, as they could not undergo MR imaging due to claustrophobia. Twelve of the 21 patients were smokers (57.14%), six were non-smokers (28.57%) and three were former smokers (14.29%). Fungal infections were diagnosed by fibrobronchoscopy with BAL in 17 patients (80.96%), open lung biopsy in two patients (9.52%) and CT-guided biopsy in two patients (9.52%). One patient died during the study period. Six patients were immunocompromised (28.57%; histoplasmosis, n=4; aspergillosis, n=2) and no patient had any cancer history.

TABLE 1 Demographic characteristics, underlying fungal infection and diagnostic method

Variable	Patients (n=21)
Age (year)[a]	58.1 (32-80)
Sex	
Male	17 (80.95)
Female	4 (19.05)
Smoking status	
Smoker	12 (57.14)
Non-smoker	6 (28.57)
Former smoker	3 (14.29)
Fungal infection	
Paracoccidioidomycosis	11 (52.38)
Histoplasmosis	4 (19.05)
Cryptococcosis	4 (19.05)
Aspergillosis	2 (9.52)
Diagnostic method	
Fibrobronchoscopy with BAL	17 (80.96)
Open lung biopsy	2 (9.52)
CT-guided biopsy	2 (9.52)
Immune status	
Immunocompromised	6 (28.57)
Immunocompetent	15 (71.43)

BAL, bronchoalveolar lavage, CT, computed tomography. Data are number of patients and percentages are in parenthesis.
[a]Data are means, with age ranges in parenthesis.

2.2 | Imaging protocols

HRCT examinations were performed using a 64-multidetector scanner (LightSpeed VCT; GE Healthcare, Waukesha, WI, USA) with the following parameters: 120 kVp; 250 mA; time, 0.8 s; and pitch, 1.375. The technical parameters included inspiratory volumetric acquisition with 1 mm collimation at 1-mm increments using a high-spatial-frequency reconstruction algorithm. Images were obtained with mediastinal (width, 350-450 HU; level, 20-40 HU) and parenchymal (width, 1200-1600 HU; level, −500 to −700 HU) window settings, and reconstructions were performed in the axial and coronal planes.

On the same day, MRI was performed using a 1.5-T scanner (Magnetom AERA; Siemens, Erlangen, Germany). For signal reception, a dedicated 08-element integrated matrix coil system that covered the whole thorax was used. This system consisted of one anterior and one posterior flexible phased-array coil, each containing a set of six receiver elements. A half-Fourier single-shot turbo spin-echo sequence was used, and the field of view was patient adapted. The sequence was performed using respiratory gating, with a navigator signal that monitored the diaphragm position. The following sequence parameters were used: repetition time (TR)/echo time (TE)/flip angle, infinite/92 ms/150°; parallel acquisition factor, 2; slice thickness, 5 mm; distance factor, 20%; transversal (matrix, 380 × 256) and coronal (matrix, 400 × 320) orientations; and acquisition time, approximately 90 s. A volumetric

interpolated breath-hold examination (VIBE) sequence was chosen for fast T1-weighted MRI. Imaging parameters for the VIBE sequence were: TR/TE, 5.12/2.51 ms; flip angle, 10°; partition thickness, 5 mm with no interslice gap; and matrix size, 256 × 116 with a three-dimensional breath-hold imaging technique. A T2-weighted fat-saturated BLADE (Siemens Medical Solutions' implementation of PROPELLER) sequence was also used, with the following imaging parameters: TR/TE, 4670/113 ms; and partition thickness, 5 mm with no interslice gap. DWI was performed using a single-shot echo-planar technique with a slice thickness of 6 mm under spectral attenuated inversion recovery (SPAIR), with respiratory-triggered scanning. The DWI parameters were: TR/TE/flip angle, 3000-4500 ms/65 ms/90°; diffusion gradient encoding in three orthogonal directions; b=0 and 800 s/mm^2; field of view, 350 mm; and matrix size, 128 × 128. The overall time spent in the MRI room was approximately 15 min. No patient required sedation.

2.3 | Imaging analysis

Two chest radiologists with more than 10 years of experience who were blinded to the patients' clinical information, except for the fungal infection, independently assessed MR and then CT images. After the two radiologists had conducted independent analyses, they reviewed the images together with a third chest radiologist (with more than 20 years of experience) to reach final consensus decisions.

Images were assessed according to criteria defined in the Fleischner Society's *Glossary of Terms*[14] and on a previous CT/MRI correlation study.[15] The following HRCT and MRI findings were evaluated: pulmonary nodules, airspace disease (consolidation and GGO), bronchiectasis, septal thickening and reversed halo sign. All findings were recorded as present or absent in each of the six pulmonary lobes (lingula was considered a pulmonary lobe). A nodule was defined as a rounded or irregular opacity that was well or poorly defined, with a diameter smaller than or equal to three centimetres. Nodules were classified as large (bigger than 1 cm in diameter) or small (smaller than 1 cm in diameter). GGO was defined as a hazy area of increased opacity or attenuation, with no obscuration of the underlying vessels. Consolidation was defined as homogeneous opacification of the parenchyma with obscuration of the underlying vessels. Bronchiectasis were characterised by bronchial dilatation with respect to the accompanying pulmonary artery, lack of tapering of bronchi and identification of bronchi within 1 cm of the pleural surface. Septal thickening was defined as clearly visible linear opacities between lobules, not normally seen in the healthy lung. Focal rounded areas of GGO surrounded by a more or less complete ring of consolidation were characterised as reverse halo sign. Findings were also categorised according to the distribution of abnormalities as unilateral or bilateral and as focal (unilobar) or diffuse (more than one pulmonary lobe).

Afterwards, reviewers identified one predominant pattern per patient for both CT and MRI examinations: nodular, airspace or reticular. A nodular pattern was characterised by the presence of innumerable discrete small, rounded opacities with diameters of 2-10 mm, with a widespread but not necessarily uniform distribution.[14] The airspace pattern has been defined as a combination of consolidation, opacity and

ground-glass appearance indicating the filling of airspaces with disease products.[14,15] A reticular pattern was defined as a collection of small linear opacities that together produce an appearance resembling a net (reticulation). Constituents of the reticular pattern were interlobular septal thickening, intralobular lines and/or cyst walls of honeycombing.[14]

Mean signal intensity of DW-MRI was analysed semiquantitatively by focusing a region of interest on each lesion with two gradient factors (bh and bl), as well as on the spinal cord at the same level. When the lesion appeared to be heterogeneous, the region of interest was placed at the location of greatest signal intensity. The lesion-to-spinal cord ratio (LSR) of signal intensity was measured on the same DW images with a diffusion gradient represented by a bh of 800 s/mm^2. A region of interest of the same size as that placed on the spinal cord was positioned on the lesion. Section locations on DW-MRI were defined by consensus. The regions of interest placed on the thoracic spinal cord were 50-76 mm^2, which was equivalent to 14-22 pixels. We used DW images with averaged multiple signal intensities obtained during quiet breathing, instead of those obtained during breath holding with no averaging of signal intensity. Accordingly, the signal-to-noise ratio was reasonably good and the LSRs obtained were reproducible.[16]

2.4 | Statistical analysis

All results were statistically analysed using commercial software (SPSS 11, SPSS Inc., Chicago, IL, USA; Excel 2007, Microsoft, Redmond, WA, USA). Using CT as the gold standard, sensitivity, specificity, positive predictive value (PPV) and negative predictive value (NPV) for MRI were calculated for each of the findings: septal thickening, airspace disease (consolidation and GGO), bronchiectasis, pulmonary nodules and reversed halo sign, according to the correspondent pulmonary region. On a second analysis focusing on the distribution of abnormalities, sensitivity, specificity, PPV and NPV for MRI were also obtained for each lobe. 95% confidence intervals (CI) were calculated for the proportions, according to Wilson score interval with continuity correction.[17] Based on the CT images, prevalences were obtained for all radiological findings. Prevalences per lobe were calculated according to the presence of any finding in the correspondent lobe.

3 | RESULTS

As no patient previously underwent lobectomies and no lung anatomy variation was observed, 126 lobes were analysed. Prevalences of each finding per lobe are summarised in Table 2. The most common predominant imaging pattern was nodular (Figure 1), found in 76.20% (n=16) of the CT scans and in 80.96% (n=17) of the MR imaging. Main reticular pattern was present in 9.52% (n=2) of CT and in 4.76% (n=1) of MR imaging (Figure 2). These heterogeneous prevalences were due to one patient that presented different predominant patterns between the two imaging modalities, with a main reticular pattern on the CT and a nodular on the MRI. Other predominant imaging presentations, reticulonodular and airspace (Figure 3), had same prevalences in both examinations (4.76% [n=1], and 9.52% [n=2] respectively). Lesions

**TABLE 2** Prevalence of findings per lobe

n=21	Findings					Overall
	Septal thickening	Airspace disease	Bronchiectasis	Nodules[a]	Reversed halo	
Right superior lobe	19.05	23.81	0	71.43	4.76	**90.48**
Middle lobe	4.76	19.05	0	42.86	0	**57.14**
Right inferior lobe	4.76	19.05	0	66.67	0	**80.95**
Left superior lobe	14.29	23.81	0	57.14	9.52	**76.19**
Lingula	4.76	14.29	0	23.81	23.81	**38.10**
Left inferior lobe	0	9.52	4.76	71.43	4.76	**71.43**
Overall	**7.94**	**19.84**	**0.79**	**55.56**	**7.14**	

Data are percentages, obtained in the computed tomography results.
[a]Nodule mean size, 6.3 mm (range, 2.5-8.0 mm).
Bold values in last line are related to the prevalence of each of the findings in any location within the lungs.
Bold values in the last column are the prevalences of any findings within each pulmonary location.
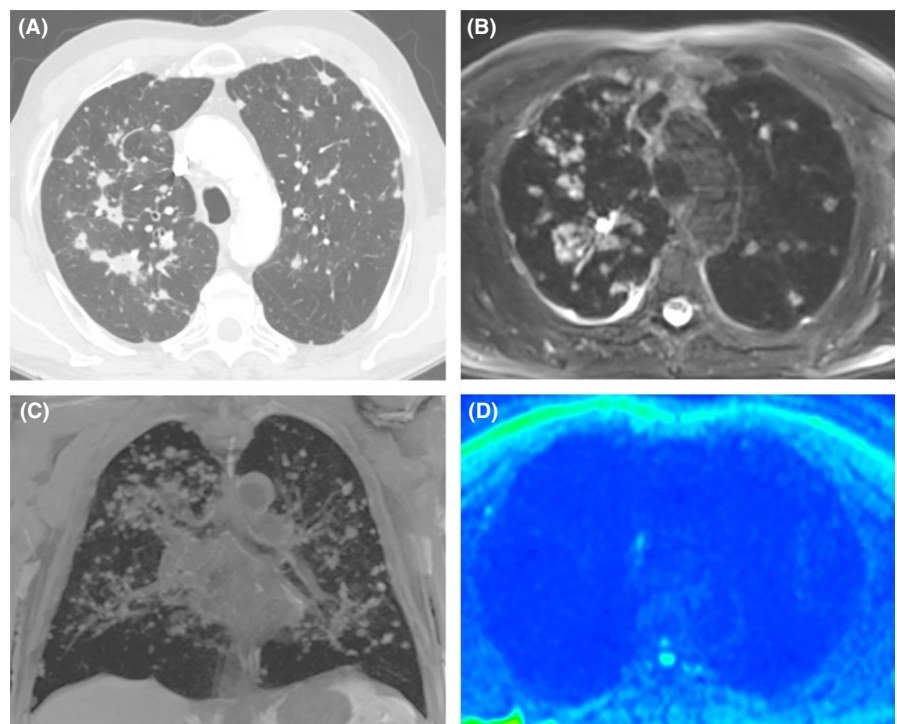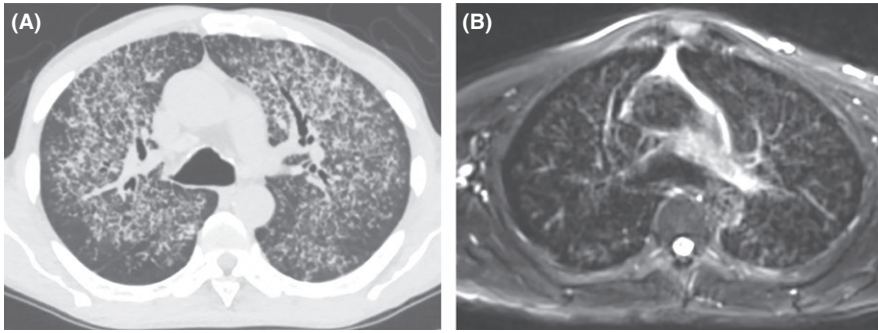

FIGURE 1 Images from a 67-year-old male with histoplasmosis and chronic cough. A, CT demonstrated diffuse centrilobular nodules in both lungs. T2 BLADE fat-saturated axial (B) and T1 VIBE coronal (C) sequences demonstrated the same findings. D, Axial diffusion-weighted sequence showing no restriction in the pulmonary nodules

were identified bilaterally in 85.70% (n=18) of patients. Among the remaining unilateral cases (n=3; 14.3%), only one presented diffuse distribution, whereas the other two had findings confined to a single lobe.

Nodules were the most common imaging finding [55.56%; mean size, 6.3 mm (range, 2.5-8.0 mm)], whereas bronchiectasis were only present in 0.79% of the 126 lobes analysed. Upper lobes were the most frequently involved pulmonary regions of each side, affecting 90.48% of the right upper lobes (RUL) and 76.19% of the left upper lobes (LUL). Otherwise, lingula was the less commonly involved site (38.10%). Despite of the lower prevalence of findings within the lingula, the reverse halo sign was more commonly found in this pulmonary region, affecting 23.81% of patients.

The results for MRI performance compared to CT and summary statistics, according to each radiological finding and to each pulmonary lobe, are summarised in Table 3. Sensitivity, specificity, PPV and NPV for MRI varied considerably according to the imaging finding and the pulmonary region. The best performance was for nodules detection (sensitivity: 100% [95% CI, 93.52-100%]; specificity: 100% [92.00-100%]; PPV: 100% [93.52-100%]; NPV: 100% [92.00-100%]). For bronchiectasis and septal thickening, MRI presented poorer positive predictive values (33.33% [95% CI, 1.77-87.47%]; and 83.33% [50.88-97.06%] respectively). Although sensitivity for bronchiectasis was high (100%), its confidence interval was quite wide (95% CI, 5.46-100%). Considering the pulmonary regions, MRI presented superior performance to identify findings in the upper lobes. For lesions in the left lower lobe, sensitivity and PPV were slightly inferior (sensitivity: 90.48% [95% CI, 68.17-98.33%]; PPV: 95% [73.06-99.74%]).

FIGURE 2 Images from a 56-year-old male with paracoccidioidomycosis and dyspnoea. A, CT on axial view demonstrated reticular patterns in both lungs, with septal thickening, ground-glass areas and bronchiectasis. B, Axial T2 BLADE fat-saturated sequence demonstrated septal thickening, with some bronchiectasis
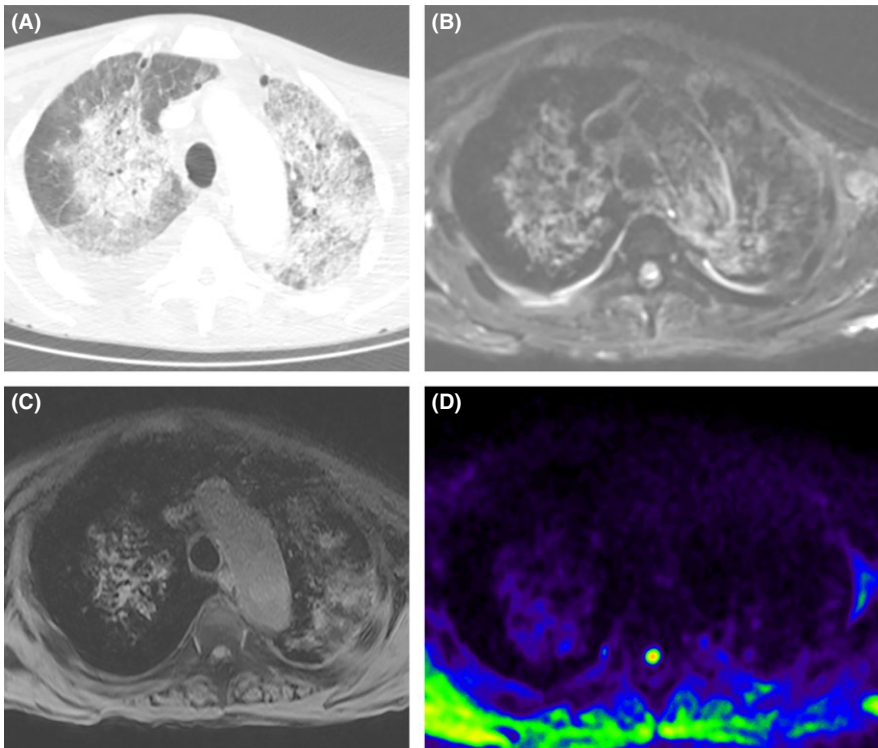
FIGURE 3 Images from an 82-year-old male with COPD and aspergillosis presenting dyspnoea, cough and fever. A, CT demonstrated diffuse pulmonary consolidations and ground-glass opacities in both lungs, some nodular opacities in the left lung, mid airway dilatation and small bilateral pleural effusions. Axial T2 BLADE (B) and T1 VIBE (C) fat-saturated sequences demonstrated areas of airspace hyperintensity signal, suggesting the airspace pattern. D, A diffusion-weighted sequence showed no restriction in abnormal areas, based on the lesion-to-spine ratio

Two false-negative cases were observed during the analysis and both presented airspace disease in the left lower lobe (LLL; Figure 4). Among the four false-positive results, two were septal thickening cases, one in the right lower lobe (RLL) and one in the LLL, and two were bronchiectasis, one in the RUL and the other in the middle lobe (ML). Further analysis revealed that both false-positive septal thickening results were in the same patient and both false-positive bronchiectasis cases were also gathered in another patient.

All DW MRI examinations were completed successfully, with no adverse effect observed. Restriction on DWI was not present in any subject. LSRs were obtained for all patients and mean LSR was 0.772 (standard deviation [SD]±0.033).

4 | DISCUSSION

Our study was designed to evaluate MRI performance to investigate pulmonary fungal diseases, compared to high-resolution CT. In a recent study, Yan et al. [18] found that the overall lesion-related

sensitivity of 3-Tesla MRI was superior to that of HRCT (90.5% vs 86.9%) in detecting invasive fungal lung infection. However, Blum et al. [19] reported that MRI was less sensitive than HRCT in the detection of initial signs of angioinvasive aspergillosis (ie halo sign). These discrepancies could be related to advances in technique and sequences over the years. Modern MRI machines enable the detection of nodular lesions as small as 5 mm (in trials and in patients with melanoma), as well as interstitial abnormalities such as septal thickening and bronchiectasis.[9] We found that results vary considerably according to the radiological finding and the pulmonary region. Specificity and negative predictive value for MRI were more reliable results due to narrower 95% confidence intervals. Although some findings and lobes presented good sensitivities and positive predictive values, 95% CI were wider, meaning greater uncertainty of these variables. These are reflexes of the small sample size, which is one of the limitations in our study.

Both false-negative results observed were airspace disease (consolidation and GGO) findings, what could be explained by the lower sensitivity of MRI compared to CT for the detection of such

TABLE 3 Summary statistics for MRI performance according to radiological finding and pulmonary lobe

	Prevalence	Sensibility	Specificity	PPV	NPV
Radiological finding					
Septal thickening	7.94	100 (65.55-100)	98.28 (93.29-99.70)	83.33 (50.88-97.06)	100 (95.94-100)
Airspace disease	19.84	92 (72.50-98.60)	100 (95.43-100)	100 (82.19-100)	98.06 (92.48-99.66)
Bronchiectasis	0.79	100 (5.46-100)	98.40 (93.76-99.72)	33.33 (1.77-87.47)	100 (96.23-100)
Nodules	55.56	100 (93.52-100)	100 (92.00-100)	100 (93.52-100)	100 (92.00-100)
Reversed halo	7.14	100 (62.88-100)	100 (96.04-100)	100 (62.88-100)	100 (96.04-100)
Pulmonary lobe					
Right superior lobe	90.48	100 (83.42-100)	98.75 (92.27-99.93)	96.15 (78.42-99.80)	100 (94.22-100)
Middle lobe	57.14	100 (73.24-100)	98.90 (93.17-99.94)	93.33 (66.03-99.65)	100 (94.90-100)
Right inferior lobe	80.95	100 (79.08-100)	98.84 (92.79-99.94)	95 (73.06-99.74)	100 (94.61-100)
Left superior lobe	76.19	100 (81.50-100)	100 (94.49-100)	100 (81.50-100)	100 (94.49-100)
Lingula	38.10	100 (73.24-100)	100 (94.95-100)	100 (73.24-100)	100 (94.95-100)
Left inferior lobe	71.43	90.48 (68.17-98.33)	98.81 (92.63-99.94)	95 (73.06-99.74)	97.65 (90.96-99.59)

NPV, negative predictive value, PPV, positive predictive value. Data are percentages and numbers in brackets are 95% confidence intervals, obtained according to Wilson score interval with continuity correction.

FIGURE 4 Images from a 56-year-old male with paracoccidioidomycosis and dyspnoea. A, CT on axial view demonstrated ground-glass opacity, most pronounced in the lingula, extending also to the left lower lobe. B, T2 BLADE fat-saturated sequence on axial view did not show this finding
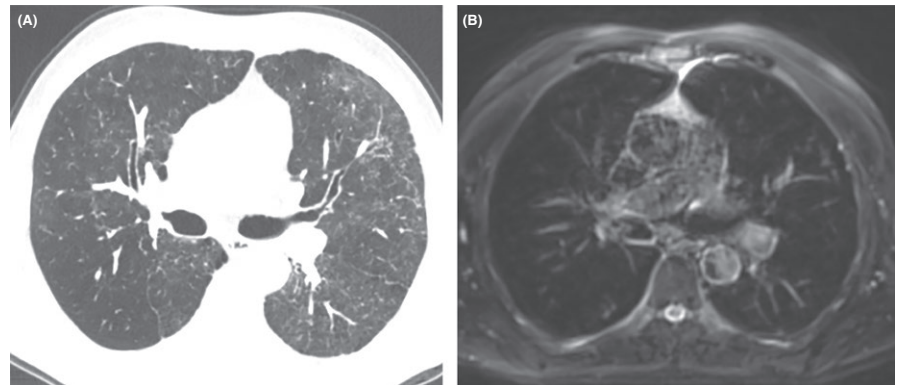
low-density lesions.[20] Both false-positive cases of septal thickening were concentrated in the same patient, such as both false-positive cases of bronchiectasis, which were also present in another same subject. These findings may suggest that false-positive results probably were related to MRI technical artefacts.

Besides the sample size, another limitation in our study was the presence of four different pathogens, what limited subgroup analysis. The size and composition of the study sample reflect the need to include patients with histopathologically confirmed fungal infection who had not undergone treatment, as it may cause cell oedema and apoptosis, modifying the DWI signal and its findings.[10,11] In addition, imaging reviewers, although blinded to clinical information, were aware of the fungal infection before assessing the examinations, what might have influenced the results.

Some studies have demonstrated the potential of DWI to differentiate malignant from benign pulmonary lesions, as malignant tumours usually present restricted diffusion.[13] In our study, restriction on DWI was not observed in any patient, what could be related to reduced special resolution of the echo planer imaging technique and free breathing diffusion-weighted imaging. However, this finding could aid the differential diagnosis of fungal lesions in oncology patients, as they

usually undergo more routine imaging studies than non-oncological patients, what might include chest MRI, performed to stage the disease, to assess the response to cancer therapy and to screen for metastasis.[21] Apparent diffusion coefficient (ADC) could bring additional information to help the differentiation between fungal infection and tumour. However, we decided not to include this measurement in our study, as a dedicated workstation would be required, what complicates ADC calculation in general practice. Alternatively, we have decided to use a simpler qualitative evaluation, the lesion-to-spine ratio, which has been demonstrated in some studies to be useful for differentiating benign and malignant lung lesions.[16,22] Uto et al. [16] found that the LSR of cancer nodules was significantly higher than that of benign lesions, with no significant differences between them in relation to ADC.

MR imaging presented superior results for specificity and NPV than for sensitivity and PPV, what indicates that a negative MRI scan would be reliable to consider stop following up these patients. This could be an alternative to multiple radiation exposures associated with CT follow-up. Further studies should aim to acquire bigger samples to sustain these results, maybe analysing patients for longer periods with both imaging modalities to validate MRI as a useful tool for follow-up rather than diagnosis of patients with pulmonary fungal infection.

CONFLICT OF INTEREST

No authors have any conflicts of interest.

REFERENCES

1. Franquet T. High-resolution computed tomography (HRCT) of lung infections in non-AIDS immunocompromised patients. *Eur Radiol*. 2006;16:707–718.
2. Roos N, Diederich S, Lentschig M, Lenzen H, Peters PE. Phenomenology of pulmonary HRCT. Definitions, differential diagnosis and clinical relevance. *Radiologe*. 1996;36:521–533.
3. Demirkazik FB, Akin AA, Uzun O, Akpinar MG, Ariyurek MO. CT findings in imunocompromised patients with pulmonary infections. *Diag Interv Radiol*. 2008;14:75–82.
4. Barreto MM, Marchiori E, Amorim VB, et al. Thoracic paracoccidioidomycosis: radiographic and CT findings. *Radiographics*. 2012;32:71–84.
5. Knox KS, Hage CA. Histoplasmosis. *Proc Am Thorac Soc*. 2010;7:169–172.
6. Lacomis JM, Costello P, Vilchez R, Kusne S. The radiology of pulmonary cryptococcosis in a tertiary medical center. *J Thorac Imaging*. 2001;16:139–148.
7. Althoff Souza C, Müller NL, Marchiori E, Escuissato DL, Franquet T. Pulmonary invasive aspergillosis and candidiasis in immunocompromised patients: a comparative study of the high-resolution CT findings. *J Thorac Imaging*. 2006;21:184–189.
8. Ackman JB, Wu CC, Halpern EF, Abbott GF, Shepard JAO. Nonvascular Thoracic magnetic resonance imaging: the current state of training, utilization and perceived value. *J Thorac Imaging*. 2014;29:252–257.
9. Biederer J, Beer M, Hirsch W, et al. MRI of the lung (1/3): methods. *Insights Imaging*. 2012;3:345–353.
10. Biederer J, Beer M, Hirsch W, et al. MRI of the lung (2/3): why... when...how? *Insights Imaging*. 2012;3:355–371.
11. Chung JH, Little BP, Forssen AV, et al. Proton MRI in the evaluation of pulmonary sarcoidosis: comparison to chest CT. *Eur J of Radiol*. 2013;82:2378–2385.
12. Koyama H, Ohno Y, Seki S, et al. Magnetic resonace imaging for lung cancer. *J Thorac Imaging*. 2013;28:138–150.
13. Satoh S, Kitazume Y, Ohdama S, et al. Can malignant and benign pulmonary nodules be differentiated with diffusion weighted MRI? *AJR*. 2008;191:464–470.
14. Hansell DM, Bankier AA, MacMahon H, et al. Fleischner Society: glossary of terms for thoracic imaging. *Radiology*. 2008;246:697–722.
15. Barreto MM, Rafful PP, Rodrigues RS, et al. Correlation between computed tomographic and magnetic resonance imaging findings of parenchymal lung diseases. *Eur J Radiol*. 2013;82:492–501.
16. Uto T, Takehara Y, Nakamura Y, et al. Higher sensitivity and specificity for diffusion-weighted imaging of malignant lung lesions without apparent diffusion coefficient quantification. *Radiology*. 2009;252:247–254.
17. Newcombe RG. Interval estimation for the difference between independent proportions: comparison of eleven methods. *Stat Med*. 1998;17:873–890.
18. Yan C, Tai X, Wei Q, et al. Lung MRI of invasive fungal infection at 3 Tesla: evaluation of five diferente pulse sequences and comparison with multidetector computed tomography (MDCT*). Eur Radiol*. 2015;25:550–557.
19. Blum U, Windfuhr M, Buitrago-Tellez C, Sigmund G, Herbst EW, Langer M. Invasive pulmonary aspergillosis. MRI, CT, and plain radiographic findings and their contribution for early diagnosis. *Chest*. 1994;106:1156–1161.
20. Lutterbey G, Gieseke J, von Falkenhausen M, Morakkabati N, Schild H. Lung MRI at 3.0T: a comparison of helical CT and high-field MRI in the detection of diffuse lung disease. *Eur Radiol*. 2005;15:324–328.
21. Hochhegger B, Marchiori E, Irion K, Souza AS Jr, Volkart J, Rubin AS. Magnetic resonance of the lung: a step forward in the study of lung disease. *J Bras Pneumol*. 2012;38:105–115.
22. Henz Concatto N, Watte G, Marchiori E, et al. Magnetic resonance imaging of pulmonary nodules: accuracy in a granulomatous disease-endemic region. *Eur Radiol*. 2016;26:2915–2920.